Journal of Sustainable Metallurgy (2019) 5:172–180
https://doi.org/10.1007/s40831-018-00207-5

THEMATIC SECTION: SLAG GRANULATION

Air-Blast Cross-Flow Atomization of Cold Fluids

Alexander Vadillo[1] · Sina Mostaghel[2,3] · Mansoor Barati[1]

Published online: 22 January 2019

Abstract
The motivation for this work is to gain a better understanding of how particle characteristic can be controlled when metallurgical slags are atomized in cross-flow air atomization. The effect of certain process parameters on the characteristics of liquid droplets produced by air-blast atomization has been investigated using water, castor oil, and glycerin. The gas-to-liquid ratio as well as the distance between the liquid and air stream were manipulated to understand their effect on the particle shape and size. The effect of liquid viscosity on the size and shape of droplets was also investigated. Droplets were observed in-flight with the use of shadow imaging, which were analyzed to provide information regarding the mentioned characteristics. It was found that a single correlation expressed as kinetic energy of the atomizing air per unit mass of the atomized liquid can explain the effects of gas/liquid ratio and distance between the air nozzle and crash point. The average particle size decreased with an increase in the gas-to-liquid flow rate ratio, increased with increasing distance between the liquid and air stream, and increased with increasing viscosity. The aspect ratio was consistent and close to unity for all water atomization experiments.

Keywords Metallurgical slag · Dry granulation · Break-up mechanism · Atomization

List of symbols

E_k	Gas kinetic energy rate (J/s)
E_s	Surface energy consumption rate (J/s)
E_n	Viscous energy dissipation rate (J/s)
m_g	Gas mass flow rate (g/s)
m_l	Liquid mass flow rate (g/s)
v_g	Gas velocity (m/s)
Δ_v	Difference between gas and liquid velocities (m/s)
ρ_l	Liquid density (g/m^3)
ρ_g	Gas density (g/m^3)
n	Number of droplets
γ	Surface tension (J/m^2)
μ	Viscosity (poise)
d_{32}	Sauter mean diameter (m)
β	Fraction of kinetic energy used to overcome surface energy
A	Impact area between gas and liquid, at the point of granulation (m^2)
A_0	Area of the air nozzle (m^2)
L	Distance between air stream and liquid stream (m)
θ	Angle of expansion (deg)

Introduction

Slag has traditionally been regarded as a waste byproduct from smelting operations and presents notable environmental, operational, and financial significance for the metallurgical industry. Typical slag generation rates range from 0.3 tonnes of slag per tonne of metal for blast furnace ironmaking to 14 tonnes of slag per tonne of metal for ferronickel production [1]. Global annual slag production is estimated at 680 million tonnes, with ferrous slags accounting for more than 90% of annual slag production at 610 million tonnes.

Conventional slag handling operations include air cooling, wet, and dry granulation. Air cooling begins with the slag being dumped into a large open area and left to cool, where in some cases it is subsequently sent to downstream crushers for further processing. Operational challenges associated with air cooling include potential emission of toxic fumes and/or possibilities of dust generation [2]. Excavation from the pit can be facilitated by

The contributing editor for this article was Sharif Jahanshahi.

✉ Alexander Vadillo
alexander.vadillo@mail.utoronto.ca

[1] Department of Materials Science and Engineering, University of Toronto, Toronto, Canada

[2] Formerly with Hatch Ltd., 2800 Speakman Dr, Mississauga, Canada

[3] Present Address: Aurubis AG, Hamburg, Germany

water spraying, which causes the slag to crystallize and crack; this requires specific safety precautions be taken to mitigate the increased risk of explosions.

Water granulation is carried out when molten slag is broken apart and quenched with a high-pressure water stream. The process has operational and environmental shortfalls, the most significant being the risk of steam explosions, the need for dewatering, and the energy costs associated with pumping and cooling large amounts of water [3]; water consumption can exceed ten times the mass of slag being atomized. The technology is also unattractive in certain areas due to water scarcity.

Dry granulation is the process of producing granules in the absence of water. Common methods of dry granulation include centrifugal granulation and air granulation. Centrifugal granulation utilizes a high-speed rotating cup or disk. Molten slag is poured into the center of the container, spreading on the surface forming a thin film that eventually breaks into slag granules. The process has been used and studied extensively; however, it has been shown to have a low production rate, high equipment and processing costs, and produces large particles [4]. The metallurgical industry has therefore been seeking alternative slag handling methods in the past five decades that address the challenges of conventional slag handling operations, namely, the ability to produce valuable slag products and the ability to recover energy from slag [5]. Air granulation has been studied since the 1980s and has demonstrated success in the production of high value slag products [6].

Air granulation, also referred to as air-blast atomization, utilizes high-velocity air to break apart and quench a stream of molten material. The process is a subset of air atomization which has been adapted for high-viscosity melts; an industrial setup installed by Hatch Ltd. is shown in Fig. 1. The process is capable of producing particles ranging from 0.5 to 5 mm [3]. The differences between air granulation and air atomization predominantly come from the geometry, relative placement, and positions of the melt and gas streams, as shown in Fig. 2. Air-blast granulation is attracting attention for treatment of different types of slag due to the fact that it is more environmentally friendly, and having lower footprint and processing costs.

It is proposed that production of powders through air atomization occurs in three distinct stages: wave growth, ligament formation, and finally the development of droplets [4]. As expected, the melt properties and operating parameters affect the final shape and size of the particles. Material properties include viscosity, density, and surface tension; operating conditions include gas to melt mass flow rate ratio, the degree of superheating, distance between the liquid and air stream, nozzle geometry, thickness of the liquid stream, and angle of impact between liquid and air.

Fig. 1 Industrial air granulation operation implemented by Hatch Ltd. (Color figure online)

The motivation for this research is to correlate shape and size of the particles to these parameters for various types of fluids and operating conditions. Cold fluid modeling with different single-phase liquids is a useful primary tool in establishing the basic correlations of air granulation. This paper presents the experimental results of the effect of the air-to-liquid ratio, the distance between the liquid and air stream, and the liquid viscosity on the shape and size of particles produced from the granulation of water, castor oil, and glycerin, which offer a range of material properties that encompass the viscosity and density of industrial slag. This research is part of an ongoing study whose goal is to fill the knowledge gap related to cross-flow air slag granulation and gain a better understanding of how the characteristics of slag granules can be controlled.

For a fixed nozzle and atomization system configuration, the dominant factor controlling particle size in air atomization is the gas-to-liquid (G/L) flow rate ratio [7]. The dynamic viscosity of the liquid being atomized also influences the final size of the particles. A study by Goudar et al. has shown that viscosity is the dominant material property influencing particle size [7]. The easiest way of altering the melt viscosity is by increasing its superheat, as shown by Small et al. [8].

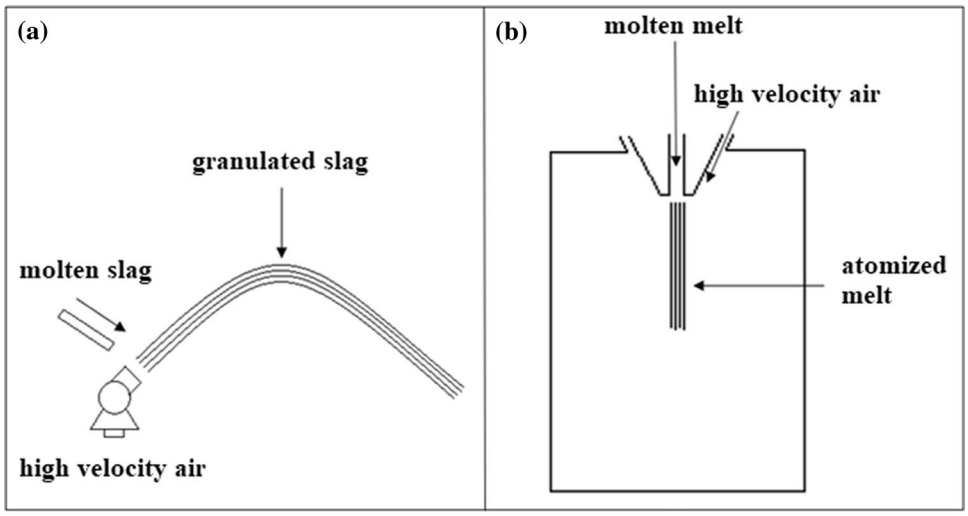

Fig. 2 **a** Air granulation setup producing slag particles, **b** Air atomization setup producing metallic powders

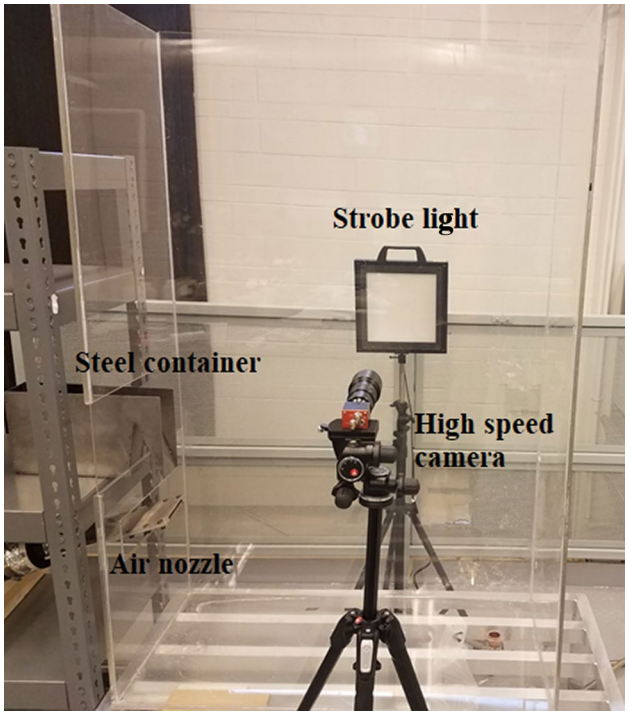

Fig. 3 Experimental setup used for cold granulation (Color figure online)

Experimental Procedure

Design of Atomization Chamber

The experimental setup used in the present study is shown in Fig. 3. The air nozzle measured 10 cm × 0.5 cm and was located below the stainless-steel container. The liquid stream was produced by allowing liquid to flow at room temperature under gravity through stainless-steel containers which produced a flowing liquid sheet with a width of either 4 or 8 cm. The air exiting the nozzle impacted the liquid sheet wherein the fluid was broken apart and dispersed as liquid particles into the granulation chamber. Liquid droplets were collected inside the chamber and drained. The granulation process was observed and photographed from the side using shadow imaging. A combination of a high-speed camera and a strobe light was used to freeze the motion of the particles for imaging and subsequent droplet shape and size analysis.

Liquid Stream Properties

Liquid flow rates were computed using the respective densities and measuring the time it took to fill a 2-L beaker. The liquid flow rates and viscosities of the single-phase liquids used in the present study are shown in Table 1.

Air Stream Properties

The axial gas velocity at the exit of the nozzle was measured using an anemometer probe. Knowing the dimensions of the nozzle allows for the computation of the gaseous mass flow rate, which are shown in Table 1.

Distance Between Air Stream and Liquid Stream

The length of the air stream represents the distance between the air nozzle and the point where granulation occurs. The setup, resulting in an air stream length of 35 cm, is shown in Fig. 4. The different lengths investigated in the present study are shown in Table 1.

Table 1 Details of the experiments conducted

Exp. no	Liquid	Liquid flow rate (g/s)	Air flow rate (g/s)	G/L ratio	Viscosity (mPa.s)	Distance between air and liquid stream (cm)	d_{32} (μm)	d_{50} (μm)
1	Water	205	20	0.10	0.89	5	860	1020
2	Water	205	40	0.2	0.89	5	730	850
3	Water	205	65	0.3	0.89	5	660	760
4	Water	125	65	0.55	0.89	5	600	720
5	Water	83	65	0.8	0.89	5	540	640
6	Water	65	65	1	0.89	5	510	610
7	Water	205	65	0.3	0.89	15	780	890
8	Water	205	65	0.3	0.89	25	1050	1200
9	Water	205	65	0.3	0.89	35	1200	1400
10	Glycerin	65	20	0.3	950	5	2060	2700
11	Glycerin	65	40	0.6	950	5	1440	1850
12	Glycerin	65	65	1	950	5	1280	1760
13	Glycerin	65	80	1.2	950	5	1100	1480
14	Glycerin	65	96	1.4	950	5	1010	1300
15	Castor Oil	40	40	1	650	5	1200	1700

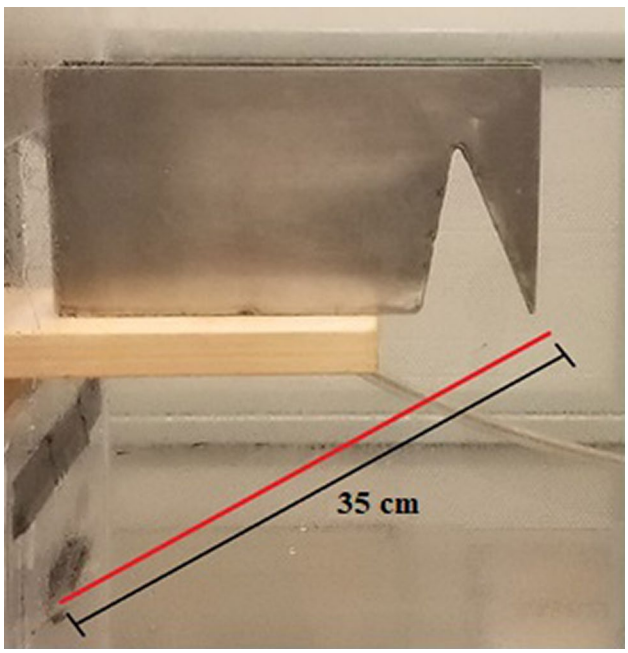

Fig. 4 Liquid container and nozzle-container arraignment (Color figure online)

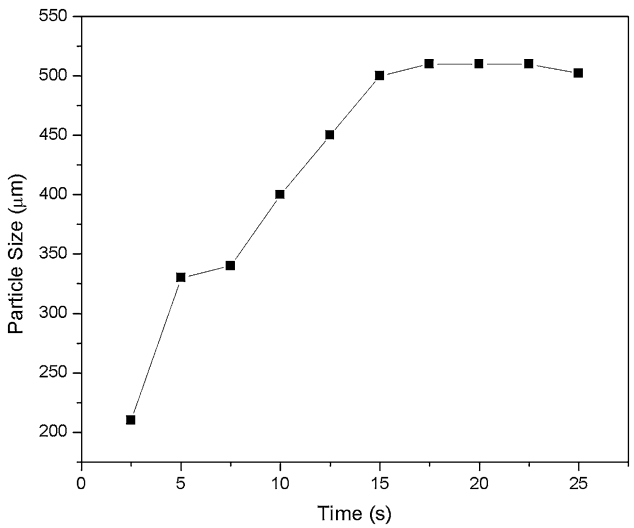

Fig. 5 Time required to achieve constant mean particle size values during the granulation of cold fluids

Characterization of Atomized Liquids

Air atomization typically produces wide particle size distributions. The particle size distribution was characterized by identifying the mean particle diameter (d_{50}, i.e., the diameter at which 50% of a samples mass is comprised of smaller particles) and the Sauter mean diameter (d_{32}, i.e., the diameter whose ratio of volume to surface area is the same as that of the entire droplet sample). For the purpose of these calculations, particles were assumed to be perfect spheres. The actual shape of particles is characterized by identifying the aspect ratio.

Image analysis was performed using ImageJ software [9], which was used to examine the shape and size of particles produced. The scale was set by using a piece of copper wire of known dimension (1.02 mm), giving a scale of 69 pixels/mm. Each experiment was repeated a minimum of two times and ran for a minimum duration of 15 s, which was identified as the time required to reach consistent d_{50} values, as shown in Fig. 5. The maximum relative

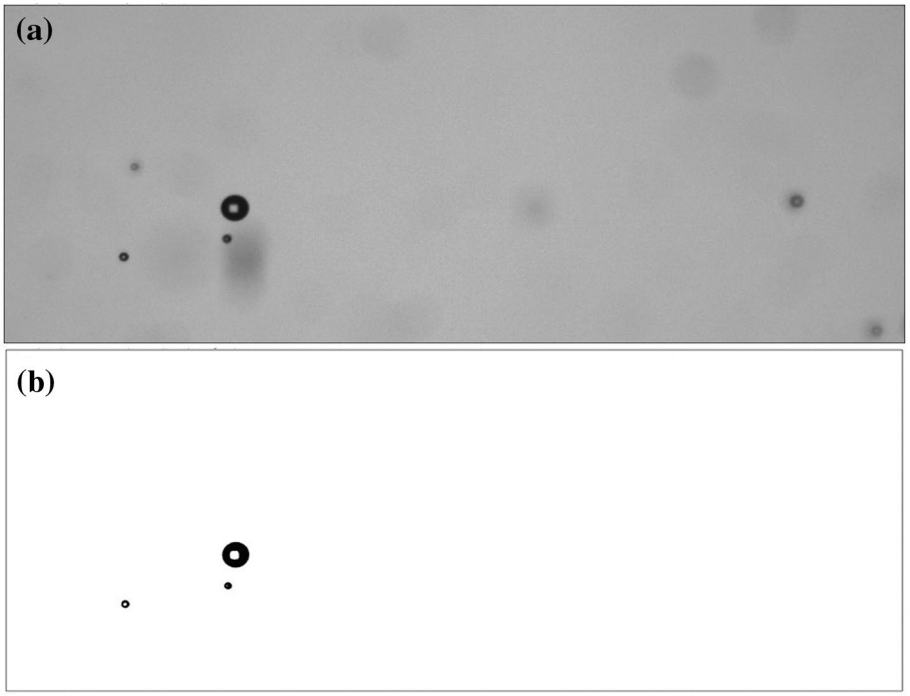

Fig. 6 Images obtained from shadow imaging **a** Pre-processing frame and **b** post-processing frame

difference between the particle sizes in repeated experiments was observed to be 7%. An example of images used for further analyses is shown in Fig. 6a. When performing the image analysis, special care was taken to remove any particles that were not in focus. An example of the same image post-processing is shown in Fig. 6b.

Results and Discussion

Theoretical Treatment

Atomization occurs as a result of the kinetic energy transfer between the gas and liquid stream. The kinetic energy is dissipated to overcome the viscous forces that resist deformation and to overcome the surface energy forces that resist the formation of new surfaces. The ratio of energy required to overcome viscous and surface tension forces, can be expressed in terms of liquid phase Weber and Reynolds numbers, Eq (1).

$$\frac{E_v}{E_s} = \frac{\mathrm{We_L}}{\mathrm{Re_L}} = \frac{\mu_l}{\gamma}\Delta v. \tag{1}$$

As the gas continues to travel after atomization, at a reduced velocity and pressure, and also the fact that gas jet is wider than the liquid sheet, it is reasonable to assume that only a certain fraction of the gas kinetic energy at the interaction point is used to overcome the surface energy forces. This fraction is denoted with the variable β in the kinetic power equation, Eq (2).

$$E_k = \frac{\beta}{2} m_g^o v_g^2. \tag{2}$$

This energy is fully consumed for break-up of the stream to a certain number of droplets. The surface energy of this particle cloud per unit time can be presented as Eq (3).

$$E_s = \pi d_{32}^2 \gamma n^o. \tag{3}$$

For a given mass flow rate of liquid, Eq (3) can be rewritten as Eq (4).

$$E_s = \frac{6\gamma m_l^o}{d_{32}\rho_l}. \tag{4}$$

To satisfy the surface energy requirements for the production of new particles, the kinetic power has to be equal to that of the surface energy created in unit time, Eq (5).

$$d_{32} = \frac{12\gamma m_l^o A^2 \rho_g^2}{\beta m_g^{o^3} \rho_l} = \frac{12\gamma}{\beta}\frac{\rho_g^2}{\rho_l}\frac{m_l^o}{m_g^{o^3}}A^2, \tag{5}$$

A schematic of the expansion of the air sheet over the length of the air stream (L) is shown in Fig. 7. The area at the point of atomization is related to the original area by Eq (6). It should be noted that the thickness of the air sheet is assumed to be much smaller than its width and it is also assumed that there is no pressure change over the short distance. The constant K′ is a relationship between

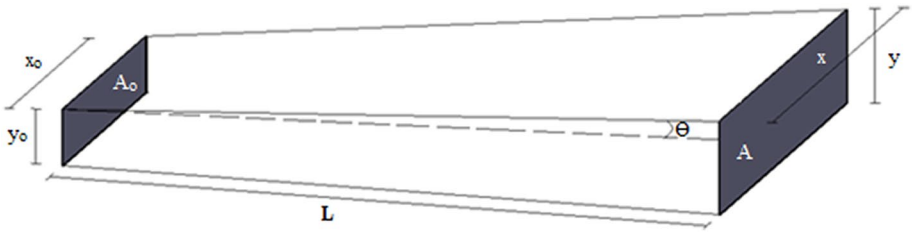

Fig. 7 Schematic of the air sheet expansion over the length of the air stream L

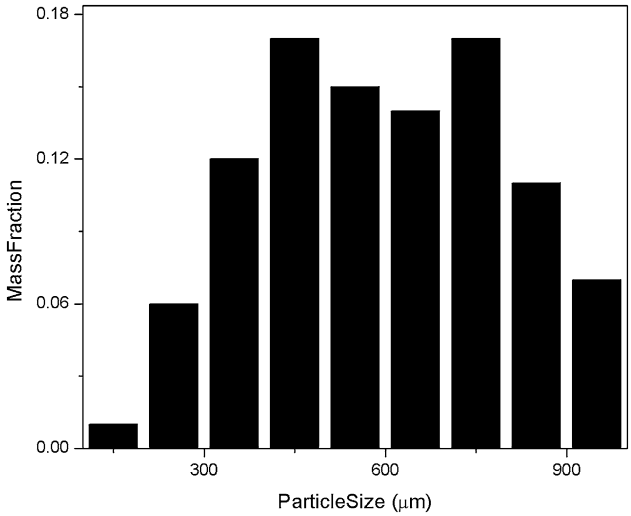

Fig. 8 Particle size distribution showing variation in mass fraction for water experiments

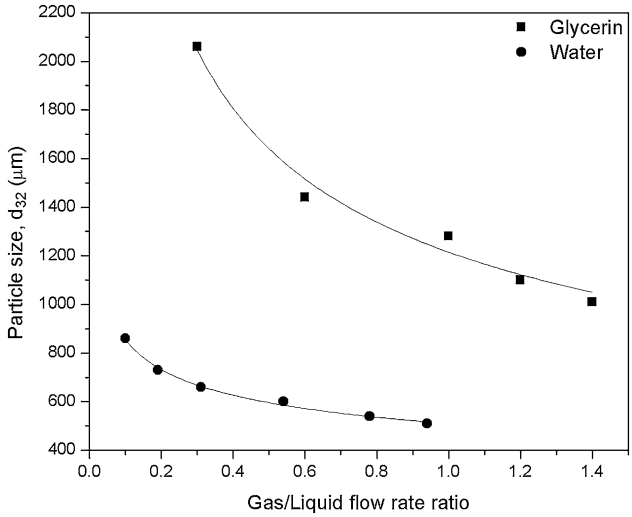

Fig. 9 Variation of mean particle size as a function of G/L flow rate ratio (Expt1–Expt14)

the angle of expansion and the original thickness of the air sheet, as shown in Eq (7). The average particle size in terms of initial operating conditions and material properties is shown in Eq (8).

$$A = A_o\left(1 + K'L\right). \tag{6}$$

$$K' = \frac{2\tan(\theta)}{y_o}. \tag{7}$$

$$d_{32} = \frac{12\gamma}{\beta}\frac{\rho_g^2}{\rho_l}\frac{m_l^o}{m_g^{o^3}}A_o^2(1 + K'L)^2. \tag{8}$$

Experimental Results

Table 1 shows the details of the experiments conducted during this study. In total, 15 different experiments were conducted at room temperature to investigate to effect of the gas-to-liquid ratio, distance between the air nozzle and crash point and the viscosity on the particle size. The mean and the Sauter mean diameter for each experiment are given in Table 1.

Effect of G/L Ratio on Particle d_{32} and Aspect Ratio

Figure 8 shows the particles size distribution of water. The mass fraction graph indicates that the majority of particles present are between 400 μm and 800 μm. Small sizes < 150 μm as well as large sizes greater than 850 μm show lower mass fractions relative to other ranges. The double-hump distribution was consistent with all the other water modeling experiments conducted in this study. This is believed to be a result of two atomization modes, the primary one with wave propagation and stream break-up and a secondary mechanism in which larger drops are broken into finer drops through an attrition-like mechanism [10, 11]. Only a portion of particles will undergo secondary atomization, causing the double-hump distribution.

Typically, the droplet size is presented versus mass flow rate ratio of gas to liquid (G/L), as shown in Fig. 9. It can be observed from the results that an increase in G/L flow rate ratio results in a decrease in the particle size. Atomization occurs as a result of kinetic energy transfer from the atomizing medium to the liquid, larger G/L ratios have a greater

kinetic energy available for sheet disintegration, resulting in smaller overall particles [12].

According to Eq. (8), when the pressure of the air stream is relatively constant, the particle size should follow a linear relationship with $m_g^{o^3}/m_l^o$. Figure 10 tests the correlation, showing that a linear trend is indeed followed.

Figure 11 shows the influence of the gas-to-liquid flow rate ratio on the particle aspect ratio. The aspect ratio describes the relationship between the width and the height of a droplet. The particle aspect ratio is dependent on the difference between the solidification time and the spheroidization time. In the present study, single-phase liquids do not undergo any solidification when atomized resulting in the droplets having ample time to spheroidize. The expected outcome was for low-viscosity liquids to spheroidize very rapidly, while liquids with a higher viscosity taking longer to spheroidize. Increasing the gas flow rate shortens the time required for droplets to spheroidize by generating smaller droplets, as shown in Fig. 11. It is important to note that for high-viscosity liquids the positioning of the camera is very important and will affect the recorded aspect ratio, it is expected that after sufficient flight time the particles will spheroidize completely.

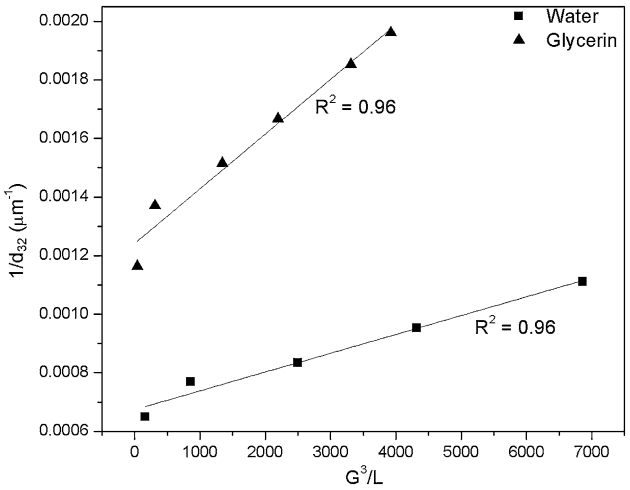

Fig. 10 Variation of the mean particle size with G^3/L flow rate ratio (Expt1–Expt14)

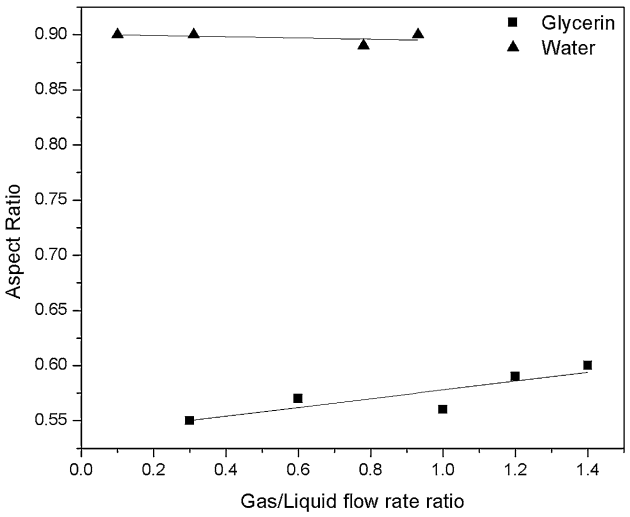

Fig. 11 Variation of aspect ratio with G/L flow rate ratio (Expt1–Expt14)

Effect of Distance Between Nozzle and Liquid Stream

Figure 12 shows the effect of the distance between air nozzle and the disintegration point. As shown, increasing the length of the air stream results in an increase in the particle size. This increase in particle size can be attributed to the loss of disintegration energy as the air has to travel a longer distance to reach the liquid stream, and also the reduction of air velocity due to expansion while traveling towards the liquid stream. This can be confirmed by looking at Eq (2), where a reduction of velocity would lead to less energy being available for granulation. As the length continues to increase, the mean particle size will increase rapidly until atomization eventually stops as the minimum kinetic energy requirements would not be met to cause any sheet disintegration.

In the present study, the particle size was related to the length of the air stream (L), by fitting the geometric parameter K′, this was then used to calculate the particle size. Figure 13 compares the calculated and measured d_{32} values with change in length of the air stream. The calculated d_{32} values are obtained by optimizing the thickness

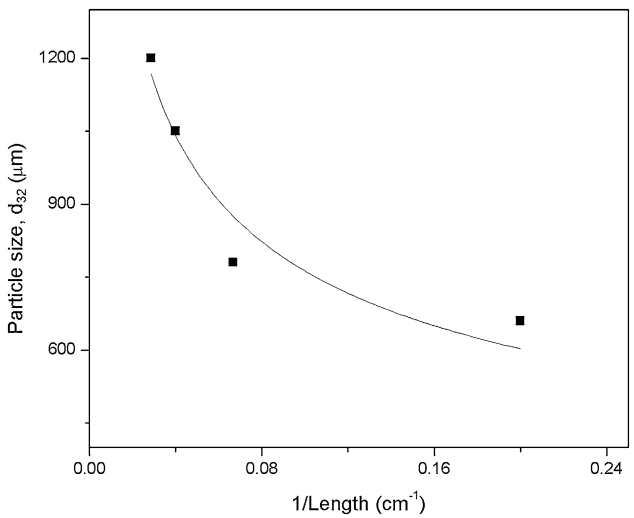

Fig. 12 Variation of mean particle size with change in length of air stream (Expts 3 and 7–9)

and the angle of expansion for the geometrical part of Eq (8):

$$d_{32} \propto A_o^2(1 + K'L)^2.$$

From the value of K′, the expansion angle of the air jet was calculated to be 0.2°. This implies very small expansion of the air stream, which is expected as the longest distance examined was 35 cm and the outlet air velocity was very high. It was also evident during the experiments that the disintegration takes place at approximately the same position of the falling liquid stream, showing little expansion of the air jet.

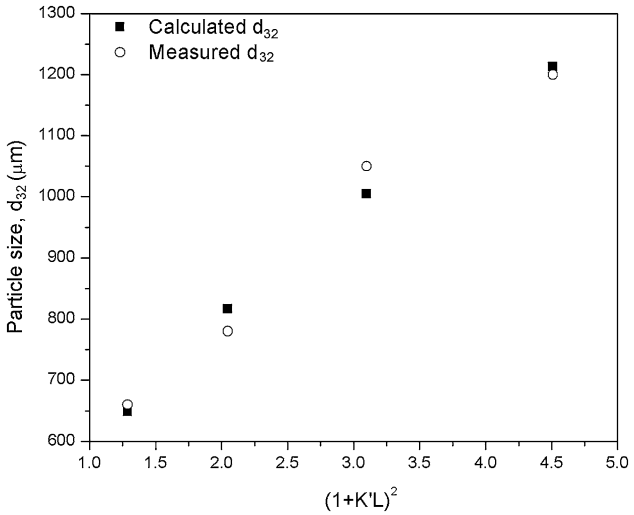

Fig. 13 Variation of the calculated and measured mean particle size with change in length of air stream

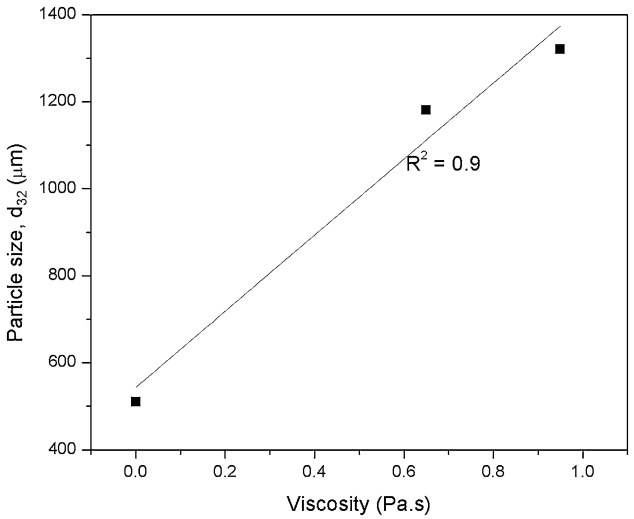

Fig. 14 Variation of mean particle size with viscosity (Expts 6, 10, and 11)

Effect of Fluid Properties

Figure 14 shows the viscosity versus the particle size for liquids with different viscosities at constant G/L flow rate ratios. Although the number of data points is not large enough to draw a quantitative correlation, it can be seen that as the viscosity increases the average particle size also increases, in what appears to be a linear relationship. This agrees with the works of Goudar et al. and Mandato et al. [7, 13]. The Sauter mean diameter for glycerin, castor oil, and water are 1280, 1200, and 510 μm, respectively. An increase in viscosity hinders disintegration leading to larger energy requirements to achieve granulation, hence the reduced particle size. This may be mathematically explained using Eq. (1) where the ratio of viscous to surface tension energies increases linearly with the liquid viscosity. The implication is that the fraction of energy consumed for disintegration which is β in Eq. (8), decreases with viscosity. This is consistent with the observed trend in Fig. 14, and subject of an ongoing study to include the effects of both viscous and surface energies into a unified correlation that would quantitatively explain the results of all experimental conditions.

Figure 15 shows the particle size distribution for glycerin; a similar distribution was observed for castor oil in Fig. 16. It can be seen that as the viscosity increases, the mass fraction tends towards a single-hump distribution, compared to the double-hump distribution for water (Fig. 8). This can be attributed to higher-viscosity liquids resisting secondary drop deformation. It is known that high-viscosity liquids exhibit a greater resistance to secondary atomization [11, 14]. The tendency is quantified using Ohnesorge number which presents the viscous forces to the inertial and surface tension forces and linearly proportional to the viscosity.

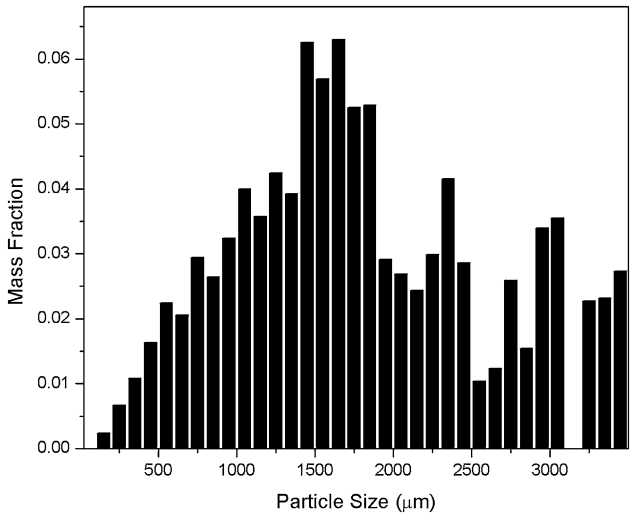

Fig. 15 Particle size distribution showing variation in mass fraction for glycerin (Expt12)

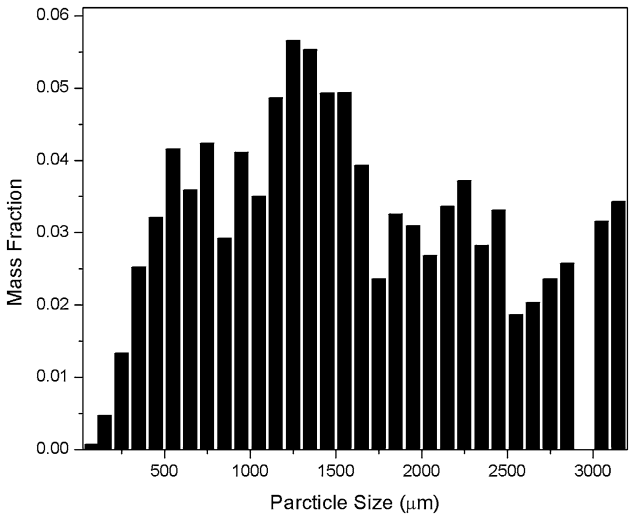

Fig. 16 Particle size distribution showing variation in mass fraction for castor oil (Expt15)

Conclusions

1. Particle size can be controlled by manipulating the G/L flow rate ratio, the length of air streams, and the viscosity of liquids.
2. Larger gas flow rate ratios produce smaller particles due to greater energy available per unit area for sheet disintegration. The particle size was related to the mass flow rate ratio of gas and liquid as m_g^3/m_l mass.
3. An increase in liquid viscosity produces a larger average particle size.
4. An increase in the distance between the air nozzle and the disintegration point produces a larger average particle size.
5. Integration of viscous and surface energies involved in liquid atomization appears to be capable of producing a quantitative correlation for prediction of particle size as function of liquid properties and operating conditions.

Acknowledgements Financial supports by OCE (Project # 23544), NSERC (Grant # CRDPJ 484828 - 15), and Hatch Ltd. are gratefully acknowledged.

References

1. Yu Q (2017) Metal recovery from steelmaking slag. University of Toronto, Toronto
2. Tasaki T (2015) Development of a cooling technology for LD-ORP slag at Nagoya Works, no. 109, pp. 155–159, 2015
3. Mostaghel S, So L, Cramer M, Faucher S, Oh SKL (2015) Slag atomising technology: unlock real value. *Fourteenth Int. Ferroalloys Congr.*, no. Energy efficiency and environmental friendliness are the future of the global ferroalloy industry, pp. 166–173, 2015
4. German RM (2005) Powder Metallurgy and Particulate Materials Processing: The Processes, Materials, Products, Properties and Applications. Metal Powder Industries Federation
5. Barati M, Esfahani S, Utigard TA (2011) Energy recovery from high temperature slags. Energy 36(9):5440–5449
6. Ando J, Onoue H, Nakahara T, Ichimura S, Kondo M (1985) Development of slag blast granulating plant characterized by innovation of the slag treatment method, heat recovery and recovery of slag as resources. Mitsubishi Heavy Ind 22:136–142
7. Goudar DM, Srivastava VC, Rudrakshi GB (2017) Effect of atomization parameters on size and morphology of Al-17Si alloy powder produced by free fall atomizer. Eng J 21(1):155–168
8. Small S, Bruce TJ (1968) The comparison of characteristics of water and inert gas atomized powders. Int J Powder Met 4(3):7–17
9. Rasband W (1997–2018) ImageJ. U. S. National Institutes of Health, Bethesda, Maryland, USA, https://imagej.nih.gov/ij/
10. Dumouchel C (2008) On the experimental investigation on primary atomization of liquid streams, pp. 371–422
11. Guildenbecher DR, López-Rivera C, Sojka PE (2009) Secondary atomization. Exp Fluids 46(3):371–402
12. Committee ASMIH (1998) 6.3 Gas Atomization. ASM handbook, Vol 07—powder metal technologies and applications. ASM International, Russel
13. Mandato S et al (2012) Liquids' atomization with two different nozzles: modeling of the effects of some processing and formulation conditions by dimensional analysis. Powder Technol 224:323–330
14. Ouyang HW, Chen X, Huang BY (2007) Influence of melt superheat on breakup process of close-coupled gas atomization. Trans Nonferrous Met Soc China 17(5):967–973